GROUP CRITICAL-TOKEN POLICY OPTIMIZATION FOR AUTOREGRESSIVE IMAGE GENERATION

Guohui Zhang[1], Hu Yu[1], Xiaoxiao Ma[1], Jinghao Zhang[1,2], Yaning Pan[3], Mingde Yao[4], Jie Xiao[1], Linjiang Huang[5], Jie Huang[1], Feng Zhao[1†]
[1]University of Science and Technology of China, [2]Shanghai Innovation Institute
[3]Fudan University, [4]The Chinese University of Hong Kong, [5]Beihang University

ABSTRACT

Recent studies have extended Reinforcement Learning with Verifiable Rewards (RLVR) to autoregressive (AR) visual generation and achieved promising progress. However, existing methods typically apply uniform optimization across all image tokens, while the varying contributions of different image tokens for RLVR's training remain unexplored. In fact, the key obstacle lies in how to identify more critical image tokens during AR generation and implement effective token-wise optimization for them. To tackle this challenge, we propose **G**roup **C**ritical-token **P**olicy **O**ptimization (**GCPO**), which facilitates effective policy optimization on critical tokens. We identify the critical tokens in RLVR-based AR generation from three perspectives, specifically: **(1)** Causal dependency: early tokens fundamentally determine the later tokens and final image effect due to unidirectional dependency; **(2)** Entropy-induced spatial structure: tokens with high entropy gradients correspond to image structure and bridges distinct visual regions; **(3)** RLVR-focused token diversity: tokens with low visual similarity across a group of sampled images contribute to richer token-level diversity. For these identified critical tokens, we further introduce a dynamic token-wise advantage weight to encourage exploration, based on confidence divergence between the policy model and reference model. By leveraging 30% of the image tokens, GCPO achieves better performance than GRPO with full tokens. Extensive experiments on multiple text-to-image benchmarks for both AR models and unified multimodal models demonstrate the effectiveness of GCPO for AR visual generation. Code is available at `https://github.com/zghhui/GCPO`

1 INTRODUCTION

Visual generative models (Sun et al., 2024; Liu et al., 2024a; Ma et al., 2024) based on the autoregressive (AR) paradigm have made significant progress in the field of high-quality image generation. Meanwhile, Reinforcement Learning (RL) with Verifiable Rewards (RLVR), demonstrated by OpenAI-o1 (OpenAI, 2024) and DeepSeek R1 (Guo et al., 2025a) to enhance the reasoning abilities of large language models (LLM) (Yang et al., 2025; Team et al., 2025), is now being gradually introduced into the visual generation to improve preference alignment and task controllability.

Recent works apply RLVR, especially Group Relative Policy Optimization (GRPO) (Shao et al., 2024) for text-to-image generation by designing visual Chains-of-Thought (CoT) (Jiang et al., 2025), optimizing reward functions (Yuan et al., 2025), and constructing customized datasets (Pan et al., 2025a). Despite these advances, these methods typically assume that each token contributes equally to the RLVR's training objective and apply uniform policy optimization across the entire image token sequence. While different tokens play distinct roles in text-to-image generation: some tokens determine and correspond to the global structure of the image, while others correspond to backgrounds or details. Concurrent RLVR-based LLM reasoning works (Wang et al., 2025d;a) also realized such a functional distinction between tokens, and split them into reasoning-related *critical tokens* and remaining knowledge-related tokens, where the former have higher entropy and dominate reasoning

[†]Corresponding author.

ability. While this analogy highlights a shared imbalance in token importance, visual generation bears higher complexity due to the causal AR modeling and bidirectional image structure.

In this paper, we identify **critical tokens** in RLVR-based AR generation from three perspectives: 1) **Causal dependency** of AR; 2) **Entropy-induced spatial structure**; and 3) **RLVR-focused token diversity**. Specifically, **1)** Early generated tokens continuously influence subsequent tokens and have a significant impact on the overall image structure due to the causal attention mechanism, as shown in Fig. 1. **2)** For the token sequence of each image, we initially attempt to correlate entropy with image token, similar to the operations in (Wang et al., 2025d). While, we find that the distribution of high/low entropy tokens didn't consistently correspond to certain parts of the image, like structure or background. Pushing one step further, we observe that the token entropy gradient map demonstrates a consistent spatial pattern among images, with the high value approximately corresponding to the structures and bridging distinct visual regions, see Fig. 2, which is sensitive to RL. **3)** Within the group of GRPO, we observe that tokens deliver varying diversities for the same position along images. As shown in Fig. 3, tokens corresponding to background and texture regions tend to exhibit higher similarity, while tokens with lower similarity correspond to more complex region structures.

On the basis of our critical token selection strategy, we introduce **G**roup **C**ritical-token **P**olicy **O**ptimization (**GCPO**), a novel RLVR framework for AR image generation that facilitates effective policy optimization on critical image tokens. During each optimization step, GCPO first selects the critical tokens following the above three perspectives. Then, we further devise a dynamic token-level advantage weight for critical tokens to better encourage exploration. This dynamic weight is based on confidence divergence of critical tokens between the updating policy model and reference model, which differs from the standard GRPO that allocates advantage uniformly for each token. Finally, we only retain the policy gradients of critical tokens to perform policy optimization.

By utilizing only critical tokens (**30%** of the tokens), GCPO achieves better performance than GRPO with full tokens on multiple text-to-image generation benchmarks. Extensive experiments demonstrate the effectiveness of GCPO, including Geneval, T2I-CompBench, and Human Preference Benchmark, which is also verified on both AR models and unified multimodal models. In summary, our contributions are as follows:

- We identify **critical tokens** in RLVR-based AR visual generation from three perspectives: Causal dependency of AR, Entropy-induced spatial structure, and RLVR-focused token diversity, achieving a structure-centric and comprehensive critical-token selection strategy.
- We propose **Group Critical-token Policy Optimization (GCPO)**, a RLVR framework for autoregressive image generation that facilitates effective policy optimization on critical image tokens. We further devise the dynamic advantage weight strategy for critical tokens to enable reasonable exploration and stabilize the inherently generative prior, based on their confidence divergence between the policy model and the reference model.
- GCPO is applicable to both AR models and unified multimodal models. Extensive experiments demonstrate that GCPO, by optimizing only critical tokens (**30%** of the tokens), achieves better performance than GRPO with full tokens across multiple T2I benchmarks.

2 Related Work

Autoregressive Visual Generation. Autoregressive image generation models (Sun et al., 2024; Team, 2024; Ma et al., 2024; Pan et al., 2025b) adopt the next token prediction paradigm, which has been widely applied in LLMs, to enable text-to-image generation. Representative works (Ramesh et al., 2022; Liu et al., 2024a) typically first use an image tokenizer (Esser et al., 2021) to discretize continuous image data into a sequence of tokens, and then employ a transformer architecture to model visual tokens. Furthermore, recent research (Huang et al., 2025) has focused on unifying image generation and image understanding within a single architecture. These models are capable of accepting diverse types of input (e.g., text, image, video) and producing one or more modalities as output. MetaMorph (Tong et al., 2024) utilizes SigLIP to extract visual embeddings and introduces modality-specific adapters for more efficient cross-modal alignment. Janus-Pro (Chen et al., 2025a) adopts a dual-encoder structure that separately processes textual and visual data. Transfusion (Zhou et al., 2024), Show-o (Xie et al., 2024), and BAGEL (Deng et al., 2025) further combine the strengths of Transformer and Diffusion architectures for multimodal understanding and generation, achieving superior performance across various tasks.

Reinforcement Learning for Visual Generation. Reinforcement Learning with Verifiable Rewards (RLVR) has achieved significant progress in the field of large language models (LLMs). A series of open-source models (Guo et al., 2025a; Team et al., 2025) and RLVR methods (Yu et al., 2025c; Yue et al., 2025; Shrivastava et al., 2025; Zeng et al., 2025a; Pan et al., 2025c) have been proposed, further advancing the development of this field. Meanwhile, recent efforts (Liu et al., 2025; Xue et al., 2025; Pan et al., 2025a) have increasingly explored the potential of RLVR, especially Group Relative Policy Optimization (Shao et al., 2024) (GRPO), in the field of visual generation. SimpleAR (Wang et al., 2025b) has demonstrated that GRPO can significantly enhance the aesthetic quality and prompt alignment of AR models. T2i-R1 (Jiang et al., 2025) leverages GRPO to jointly optimize both semantic-level and token-level Chain-of-Thought (CoT) reasoning processes, thereby improving the generative capabilities of a unified multimodal model. In addition, (Gallici & Borde, 2025) introduces GRPO into scale-wise visual generative models that achieve high-quality image generation by predicting the “next scale” and demonstrating great potential (Han et al., 2025).

Reinforcement Learning for Critical tokens. Recently, several studies (Li et al., 2025; Vassoyan et al., 2025; Wang et al., 2025c; Zhao et al., 2025; Zeng et al., 2025b; Ma et al., 2025) have focused on the deeper analysis and exploration of the role of RL in LLMs’ reasoning task, especially at the token level. Critical Tokens Matter (Lin et al., 2024) suggests that identifying and replacing critical tokens can significantly improve the model’s accuracy, and proposes a contrastive estimation method to accurately locate these tokens. ConfPO (Yoon et al., 2025) further investigates the effectiveness of selectively optimizing only low-confidence and information-rich tokens. Additionally, (Wang et al., 2025d;a) points out the existence of “fork” tokens in LLM reasoning paths, indicating that these tokens typically have high entropy and are related to logical reasoning. They further observe that these fork tokens (critical tokens) can be identified by entropy and play more critical role than other tokens in enhancing the LLM’s reasoning ability. However, identifying critical tokens in AR visual generation and implementing effective token-wise optimization for them remains unexplored.

3 PRELIMINARY

Autoregressive Image Generation. A common autoregressive (AR) model includes two main components: an image tokenizer and an AR transformer (Esser et al., 2021; Yu et al., 2021; 2025b;a). For image tokenizer, typically VQ-VAE (Van Den Oord et al., 2017), it converts images $\mathcal{I} \in \mathcal{R}^{H\times W\times 3}$ into discrete tokens sequence $Z = \{z_1, \dots, z_N\}$, where each token $z_t \in \mathcal{V}$. $\mathcal{V}$ and t represent the VQ-VAE codebook and token index in sequence, respectively. Next, the AR model autoregressively predicts the joint distribution of the next image token conditioned on the text and previously generated tokens: $P(z|c) = \prod_{t=1}^{N} P(z_t|z_{<t}, c)$, where c represents text embedding.

Token Entropy. The AR model outputs probability distribution over the codebook $\mathcal{V}$ for each token. Therefore, we can use the following formula to calculate the entropy (Shannon, 1948) of this distribution, which is referred to as the token entropy H:

$$H(z_t) = -\sum_{k=1}^{V} P_{t,k} \log P_{t,k}. \tag{1}$$

Group Relative Policy Optimization (GRPO). For each prompt p, GRPO (Shao et al., 2024) samples a group of image outputs $\{o^1, o^2, \dots\}$ from the old policy model $\pi_{\theta_{old}}$. Then, it computes the corresponding rewards $\{r^1, r^2, \dots\}$ for each output within each group. The advantage A^i is calculated from the rewards of the group, and each output in the group shares the same advantage. Then optimizes the policy model $\pi_{\theta_{old}}$ by maximizing the following objective:

$$\mathcal{J}_{\text{GRPO}}(\theta) = \mathbb{E}_{\{o^i\}_{i=1}^{G} \sim \pi_{\theta_{\text{old}}}}$$

$$\left[\frac{1}{G} \sum_{i=1}^{G} \frac{1}{|o^i|} \sum_{t=1}^{|o^i|} \left(\min\left(r_t^i(\theta) \hat{A}^i, \text{clip}\left(r_t^i(\theta), 1-\varepsilon, 1+\varepsilon \right) \hat{A}^i \right) - \beta D_{\text{KL}}(\pi_\theta \| \pi_{\text{ref}}) \right) \right], \tag{2}$$

where

$$A^i = \frac{r^i - mean(\{r^1, r^2, \cdots, r^G\})}{std(\{r^1, r^2, \cdots, r^G\})}, \quad r_t^i(\theta) = \frac{\pi_\theta(o_t^i \mid q, o_{<t}^i)}{\pi_{\theta_{\text{old}}}(o_t^i \mid q, o_{<t}^i)}. \tag{3}$$

4 Observation and Analysis in AR Visual Generation

4.1 Causal dependency of AR

The core capability of AR models stems from the causal attention mechanism in transformers. Under this next token prediction paradigm, the initially generated tokens continuously influence the generation of all subsequent tokens, thereby significantly impacting the overall structure and layout of the image. To further validate this point, we inject additional noise into the tokens at different positions during the generation process (Beyer et al., 2025). This causal influence is visibly illustrated in Fig. 1, where perturbations to the early 58 tokens (token index from 0 to 58) introduce substantial changes to the image's global structure, while perturbations to the middle 58 tokens (token index from 250 to 308) only affect local details. This empirical evidence confirms that early tokens serve as global priors and structural guides. In contrast, later tokens are constrained by both preceding tokens and local consistency, making them more focused on generating local content and details. Therefore, the initial tokens should be part of critical tokens, as these early decisions propagate throughout the entire AR generation and establish the foundation for high-quality visual structures.

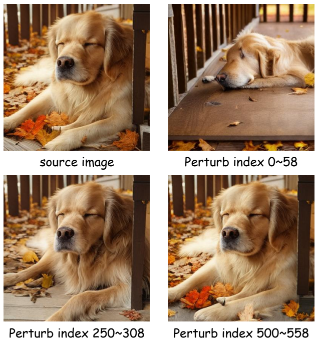

Figure 1: Visual results of perturbing different tokens.

4.2 Entropy-induced spatial structure

Concurrent RLVR-based LLM reasoning works (Wang et al., 2025d;a) have found a functional distinction between text tokens, and split them into reasoning-related critical tokens and knowledge-related tokens based on *token entropy*. The former with high entropy (such as "wait", "however") serve as logical **connectors** that bridge consecutive reasoning parts in CoT, while the latter with low entropy primarily capture factual or domain-specific knowledge.

Inspired by this, we first analyze the entropy distribution of image tokens. As shown in Fig. 2, we observe that the distribution of high/low entropy tokens corresponds to different parts of the image in different prompts: tokens with high entropy mainly correspond to the background in Fig. 2 (a), while corresponding to the subject in Fig. 2 (b). This phenomenon gradually becomes obvious in RL training. We argue that it is likely influenced by image and prompt complexity, and we provide more analysis results in Sec. B. Furthermore, we find that this entropy distribution in images exhibits a regional and spatial pattern, where tokens within the subject or background regions have approximate entropy values. We argue that image tokens exhibit strong spatial locality, with neighboring pixels sharing similar visual characteristics and entropy values (He et al., 2024; Xiang & Fan, 2025).

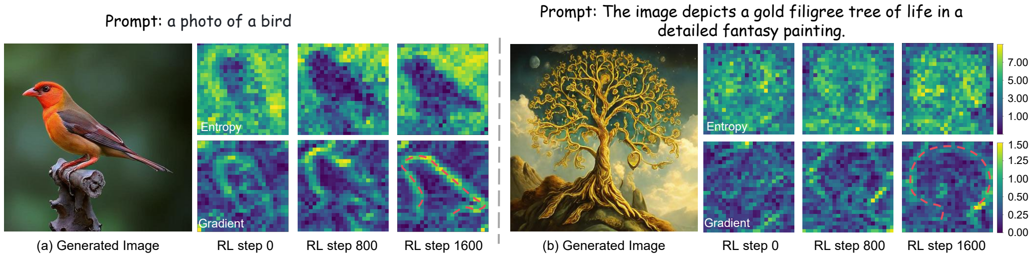

Figure 2: The entropy maps of images exhibit distinct spatial patterns. Tokens with high entropy gradient consistently correspond to image structure, which gradually strengthens with RL training.

Pushing one step further, we analyze the 2D gradient of entropy and observe consistent spatial patterns among different images. Specifically, tokens with high entropy gradients typically correspond to subject structure or regions with significant structural variation, and this pattern becomes more pronounced with RL training. These tokens exhibit large entropy changes in neighboring tokens, serving as **connectors** to link distinct visual regions. Based on this insight, we point out that tokens with high entropy gradients are critical and sensitive for spatial structures, and entropy gradients can serve as a universal and reliable proxy for identifying tokens associated with image structure.

4.3 RLVR-FOCUSED TOKEN DIVERSITY

GRPO typically relies on sample-level reward signals, where the differences between samples guide the direction of policy optimization. A group of similar samples provides limited reward information, which restricts the model's performance improvement and training efficiency. In light of this, (He et al., 2025; Yu et al., 2025c; Chen et al., 2025b) focus on enhancing sample diversity through entropy regularization or encouraging semantic diversity. In AR visual generation task, we further focus on token-level diversity. Within the group of GRPO, we observe that tokens deliver varying diversities for the same position along images. As shown in Fig. 3, tokens in background and texture regions tend to exhibit higher similarity and hardly reflect the visual differences among images. While tokens with lower similarity correspond to more complex regional structures and contribute to richer information for GRPO-based policy optimization. Therefore, we select tokens with low similarity as part of critical tokens.

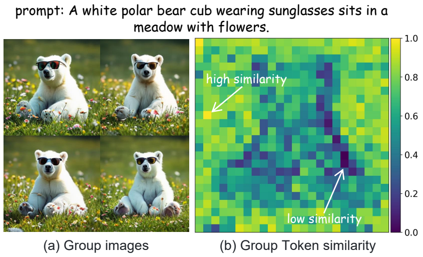

(a) Group images (b) Group Token similarity

Figure 3: The average cosine similarity of tokens at corresponding location across a group of images.

4.4 DYNAMIC ADVANTAGE WEIGHT

Balancing exploration with stabilization of generative priors is crucial for different tokens during RLVR training (Wang et al., 2025a). We argue that different critical tokens should have dynamic and distinct exploration constraints. Specifically, initial tokens should explore more moderately to prevent global structural collapse, while tokens with high entropy gradients and low similarity should have stronger exploration. Considering that the reference model itself serves as the starting point for training, we analyze the confidence divergence of each token between the training policy model and the reference model. As shown in Fig. 4, we observe that this divergence is not only dynamic as the policy model updating, but also has distinct constraints: initial tokens exhibit smaller confidence divergence, while tokens corresponding to structures show larger divergence. Based on this, we utilize this dynamic divergence as weight to eliminate complex manual specification.

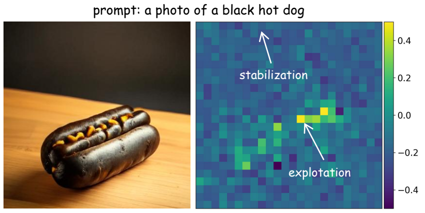

Figure 4: Confidence divergence between the Policy and Reference model

5 GROUP CRITICAL-TOKEN POLICY OPTIMIZATION

5.1 TOKEN SELECTION

The Sec. 4 discusses the critical image tokens selection from three aspects. Here, we detail the token selection strategy, as illustrated in Fig. 5. Specifically, we denote the image token sequence as $Z = \{z_1, \ldots, z_N\}$, where N is the total length of the sequence. The initial image tokens is represented as $Z_{init} = \{z_1, \ldots, z_{K_{init}}\}$, with K_{init} indicating the number of initial tokens.

Subsequently, we reshape the entropy sequence $\{H_t\}_{t=1}^{N}$ associated with these tokens into a 2D entropy map to select structure-related tokens. To mitigate the influence of noise in the entropy map, we perform a local averaging operation. Considering the local spatial and causal dependency of image tokens, the averaging is performed as follows:

$$\bar{H}_t = mean(H_t + H_t^{(l,u)} + H_t^{(u)} + H_t^{(r,u)} + H_t^{(l)}), \tag{4}$$

where (l, u), (u), (r, u) and (l) denote the upper-left, upper, upper-right and left neighboring positions of H_t, respectively. Then, we use the central difference to calculate the gradient of each token in the average entropy map. We select the K_{struct} tokens with the largest gradients as Z_{struct}.

Next, we calculate the cosine similarity of token embeddings at each sequence position within group of images. Specifically, for each token sequence position t, we consider the group of token embeddings $\{e_{t,1}, e_{t,2}, \ldots, e_{t,G}\}$ derived from G images. The pairwise cosine similarity between token

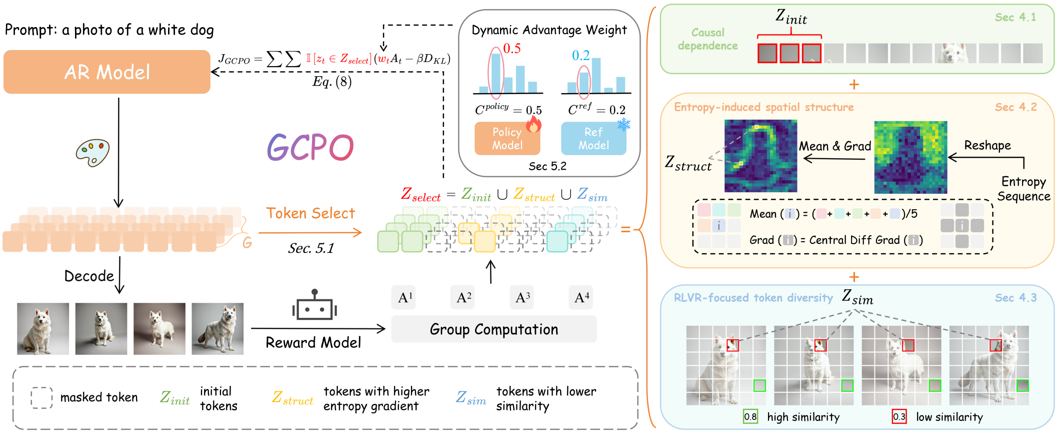
Prompt: a photo of a white dog
AR Model
$J_{GCPO} = \sum\sum \mathbb{I}[z_t \in Z_{select}](w_t A_t - \beta D_{KL})$
Eq. (8)
GCPO
Dynamic Advantage Weight
0.5
0.2
$C^{policy} = 0.5$
$C^{ref} = 0.2$
Policy Model
Ref Model
Sec 5.2
G
Token Select
Sec. 5.1
$Z_{select} = Z_{init} \cup Z_{struct} \cup Z_{sim}$
=
Decode
Reward Model
A¹
A²
A³
A⁴
Group Computation
masked token
Z_{init} initial tokens
Z_{struct} tokens with higher entropy gradient
Z_{sim} tokens with lower similarity
Z_{init}
Causal dependence
Sec 4.1
+
Entropy-induced spatial structure
Sec 4.2
Z_{struct}
Mean & Grad
Reshape
Entropy Sequence
i
Mean (i) = (+ + + +)/5
Grad (i) = Central Diff Grad (i)
+
RLVR-focused token diversity
Z_{sim}
Sec 4.3
0.8 high similarity
0.3 low similarity

Figure 5: **Overview of GCPO.** GCPO first generates a group of images for each prompt and obtains the corresponding reward. For token selection, we first select the initial token as Z_{init}. Then, we calculate the local mean and central difference gradient in 2D entropy map, and select the token with the higher gradients as Z_{struct}. Subsequently, we select the tokens with lower similarity as Z_{smi} based on intra-group cosine similarity at each position. For dynamic advantage weight, we calculate the cumulative mean confidence difference of each token as the advantage weight w_t. Finally, we only retain the policy gradients of critical tokens Z_{select} to perform policy optimization.

embeddings at position t is calculated as follows:

$$S_{jk}^{(t)} = \frac{e_{t,j} \cdot e_{t,k}}{\|e_{t,j}\|\|e_{t,k}\|}, \quad 1 \le j < k \le G. \tag{5}$$

We then calculate the average pairwise similarity $\bar{S}_t$ for each sequence position t. We select the $K_{\text{similarity}}$ tokens with the lowest average based on $\bar{S}$.

Finally, the overall critical token selection set is defined as the union of the three subsets:

$$Z_{select} = Z_{init} \cup Z_{struct} \cup Z_{sim}. \tag{6}$$

By default, the size of each subset K_{init}, K_{struct}, and K_{sim} is set to 10% of the total token sequence length, ensuring balanced and representative selection.

5.2 Dynamic Advantage Weight

The Sec. 4.4 discusses the motivation of the dynamic advantage weight. Furthermore, considering that the token at position t is predicted by its preceding tokens, we further employ the cumulative average of confidence divergence as the weight for each critical token. This can be formalized as:

$$w_t = \frac{1}{t} \sum_{j=1}^{t} clip\left(C_j^{policy} - C_j^{ref}, -\epsilon_w, \epsilon_w\right), \tag{7}$$

where w_i denotes the advantage weight at position t. C_j^{policy} and C_j^{ref} represent the confidence (model's log probability) of the j-th token on the policy model and the reference model, respectively. ϵ_w is the clip coefficient to prevent excessive weights from influencing training stability.

5.3 Objective Function

The overall objective of GCPO is formulated as follows:

$$\mathcal{J}_{\text{GRPO}}(\theta) = \mathbb{E}_{\{o^i\}_{i=1}^G \sim \pi_{\theta_{\text{old}}}} \left[\frac{1}{G} \sum_{i=1}^{G} \frac{1}{|o^i|} \sum_{t=1}^{|o^i|} \mathbb{I}\left[z_t \in Z_{select}\right] \left(w_t^i \min\left(r_t^i(\theta) \hat{A}^i, \right.\right.\right.$$
$$\left.\left.\left. \text{clip}\left(r_t^i(\theta), 1-\varepsilon, 1+\varepsilon\right) \hat{A}^i \right) - \beta \mathbb{D}_{\text{KL}}(\pi_\theta \| \pi_{\text{ref}}) \right) \right], \tag{8}$$

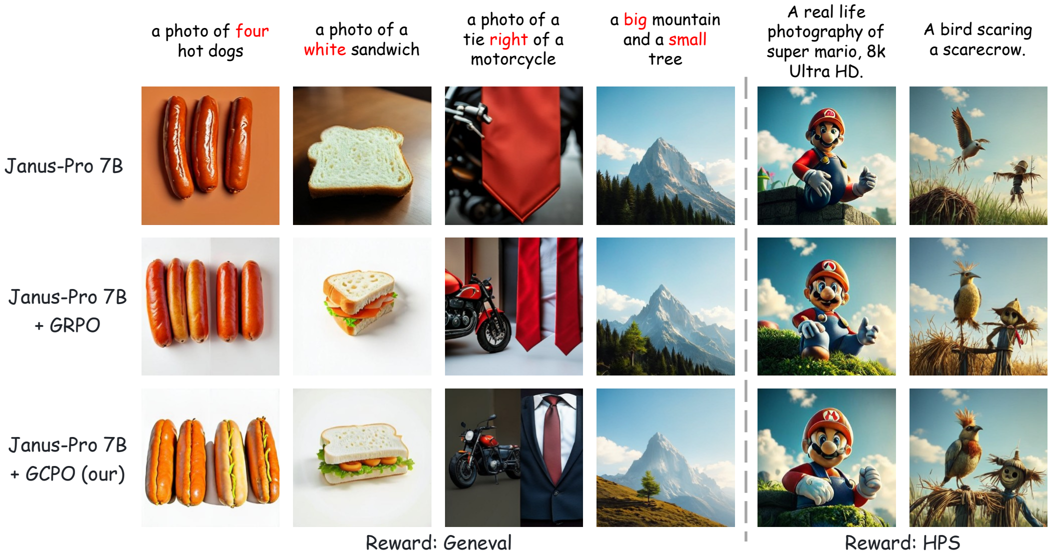
a photo of four hot dogs
a photo of a white sandwich
a photo of a tie right of a motorcycle
a big mountain and a small tree
A real life photography of super mario, 8k Ultra HD.
A bird scaring a scarecrow.
Janus-Pro 7B
Janus-Pro 7B + GRPO
Janus-Pro 7B + GCPO (our)
Reward: Geneval
Reward: HPS

Figure 6: Visualization Results. We provide image generation results on Counting, Color, Position, and Shape tasks, as well as image quality.

where $\mathbb{I}[\cdot]$ is the indicator function that evaluates to 1 if the condition inside holds and 0 otherwise.

The differences are highlighted in red between Equation (8) and Equation (3): **(i)** The optimization term of each token is multiplied by $\mathbb{I}\left[z_t \in Z_{select}\right]$, ensuring that only critical tokens in Z_{select} are involved in the overall optimization objective; **(ii)** The advantage term of each critical token is multiplied by w_t, allocating token-wise advantage weight to encourage exploration.

6 Experiments

In this section, we evaluate GCPO to improve the performance of AR model and the unified multi-modal model on two representative tasks. (1) Composition Image Generation: We report the results on GenEval and T2i-Compbench, which primarily evaluate the models' ability on spatial relationships and color attributes. (2) Image quality and Human Preference Alignment: We report DEQA, ImageReward, and PickScore metrics, reflecting the visual quality and human preference of images.

6.1 Experimental Setup

Training Settings. For the composition image generation task, our training dataset is sourced from 50,000 training prompts generated by Geneval pipeline, following (Liu et al., 2025). For the image quality and human preference alignment task, we utilize 15000 prompts from the HPSv2 training dataset. We conduct evaluations on LlamaGen (Sun et al., 2024), Janus-Pro 1B (Chen et al., 2025a), and Janus-Pro 7B (Chen et al., 2025a). Please refer to the Appendix A for detailed training settings.

Benchmark. We evaluate our method on Geneval (Ghosh et al., 2023), T2I-CompBench (Huang et al., 2023), and DrawBench (Saharia et al., 2022) to comprehensively validate effectiveness. T2I-CompBench is a comprehensive benchmark for open-world compositional text-to-image generation, covering six compositional task categories. DrawBench contains comprehensive and challenging prompts designed to assess the generative capabilities of T2I models. We use it to evaluate DEQA-Score (You et al., 2025), ImageReward (Xu et al., 2023) and Pick Score (Kirstain et al., 2023) metrics. We also report HPSv2 score (Wu et al., 2023) on HPSv2 Benchmark test data.

Reward Model. For the composition image generation task, following (Liu et al., 2025), we adopt Geneval reward as our reward model. For the image quality and human preference alignment task, we use HPSv2 as our reward model. Notably, given the relatively lower performance of LlamaGen on Geneval, we only use HPSv2 as the reward model for this base.

Table 1: Quantitative comparison results on the GenEval benchmark. The best result is in green .

Method	Overall↑	Sing Obj.↑	Two Obj.↑	Counting↑	Color↑	Position↑	Color Attr.↑
Diffusion-based Method							
PixArt-α (Chen et al., 2024)	0.48	0.98	0.50	0.44	0.80	0.08	0.07
SDXL (Podell et al., 2023)	0.55	0.98	0.74	0.39	0.85	0.15	0.23
SD3 (Esser et al., 2024)	0.63	0.98	0.78	0.50	0.81	0.24	0.52
DALL-E 3 (Betker et al., 2023)	0.67	0.96	0.87	0.47	0.83	0.43	0.45
FLUX.1-dev (Labs, 2024)	0.66	0.98	0.81	0.74	0.79	0.22	0.45
AR-based method							
LlamaGen (Sun et al., 2024)	0.32	0.71	0.34	0.21	0.58	0.07	0.04
Emu3 (Wang et al., 2024)	0.54	0.98	0.71	0.34	0.81	0.17	0.21
Show-o (Xie et al., 2024)	0.68	0.98	0.80	0.66	0.84	0.31	0.50
GPT-4o (OpenAI, 2025)	0.85	0.99	0.92	0.85	0.91	0.75	0.66
Janus-Pro-1B (Chen et al., 2025a)	0.73	0.98	0.82	0.51	0.89	0.65	0.56
Janus-Pro-7B (Chen et al., 2025a)	0.80	0.99	0.89	0.59	0.90	0.79	0.66
AR-based Method + RL							
Show-o+PARM (Guo et al., 2025b)	0.69	0.97	0.75	0.60	0.83	0.54	0.53
T2I-R1 (Jiang et al., 2025)	0.79	0.99	0.91	0.53	0.91	0.76	0.65
LlamaGen+GRPO	0.39	0.83	0.41	0.28	0.68	0.11	0.06
Janus-Pro-1B+GRPO	0.84	1.00	0.95	0.59	0.84	0.88	0.77
Janus-Pro-7B+GRPO	0.87	0.99	0.92	0.71	0.94	0.92	0.73
Our							
LlamaGen+GCPO	0.42	0.83	0.49	0.25	0.71	0.13	0.08
Janus-Pro-1B+GCPO	0.85	1.00	0.96	0.63	0.88	0.91	0.73
Janus-Pro-7B+GCPO	0.90	0.99	0.95	0.90	0.90	0.95	0.76

Table 2: Comparison results on T2I-CompBench and DrawBench, evaluated by DEQA-Score, ImageReward, and PickScore. The best result is in green . Time: Time consumption of each RL-training step. We achieve state-of-the-art performance without introducing additional time overhead.

Method	Color↑	Shape↑	Texture↑	Spatial↑	Non-Spat.↑	Complex↑	DEQA↑	HPS↑	ImgRwd↑	PickScore↑	Time (s)↓
AR-based method											
LlamaGen (Sun et al., 2024)	0.4202	0.3967	0.5103	0.0772	0.3050	0.2908	2.70	21.62	-0.36	20.27	-
Janus-Pro-1B (Chen et al., 2025a)	0.3439	0.2363	0.2788	0.0969	0.2813	0.2733	3.38	25.46	-0.19	20.79	-
Janus-Pro-7B (Chen et al., 2025a)	0.6359	0.3528	0.4936	0.2061	0.3085	0.3559	3.55	28.00	0.68	21.82	-
AR-based Method + RL											
LlamaGen+GRPO	0.4454	0.4092	0.5446	0.0780	0.3069	0.3066	2.85	25.28	-0.14	20.44	7.63
Janus-Pro-1B+GRPO	0.7050	0.3150	0.4621	0.3020	0.2963	0.3159	3.67	29.16	0.73	21.59	9.54
Janus-Pro-7B+GRPO	0.7478	0.3999	0.5849	0.2481	0.3090	0.3744	3.70	30.64	0.99	22.12	14.75
Our											
LlamaGen+GCPO	0.4691	0.4351	0.5726	0.1015	0.3086	0.3199	2.97	26.27	0.10	20.59	7.69
Janus-Pro-1B+GCPO	0.7373	0.3201	0.4803	0.3220	0.2948	0.3059	3.73	29.61	0.73	21.60	9.69
Janus-Pro-7B+GCPO	0.7508	0.5173	0.7030	0.3824	0.3133	0.3888	3.73	30.90	1.01	22.10	14.89

6.2 Main Results

We compare our method with leading AR models and diffusion models on GenEval, as shown in Table 1. Only utilizing critical tokens (30% of the total tokens), GCPO achieves significant improvements over GRPO across all three base models. Notably, Janus-Pro-7B+GCPO attained the highest overall score of **0.90**. This is primarily attributed to a substantial improvement in the Counting task (+0.19). Furthermore, Table 2 shows results of our method on T2I-CompBench, which differs substantially from the GenEval-style training data. GCPO consistently outperforms GRPO in the majority of tasks, achieving up to 20% performance gains on Shape (+0.1174), Texture (+0.1181), and Spatial task (+0.1343), thereby demonstrating strong generalization. We analyze the time consumption of our method in Table 2. Our approach achieves the aforementioned performance gains without introducing additional computational overhead (GCPO only increases time consumption by 1%). As shown in Fig. 6, the model with our method accurately understands the shape of the mountain (big) and the tree (small). In contrast, the model with GRPO generates a forest.

As shown in Table 2, under the HPS-based reward setting, our method consistently outperforms GRPO and demonstrates superior performance across all three models. Notably, Janus-Pro-7B+GCPO achieves the best scores on image quality and human preference alignment. Meanwhile, the images generated by our method exhibit more natural and vivid details, as illustrated in Fig. 6. For more comparison results, please refer to Appendix F.

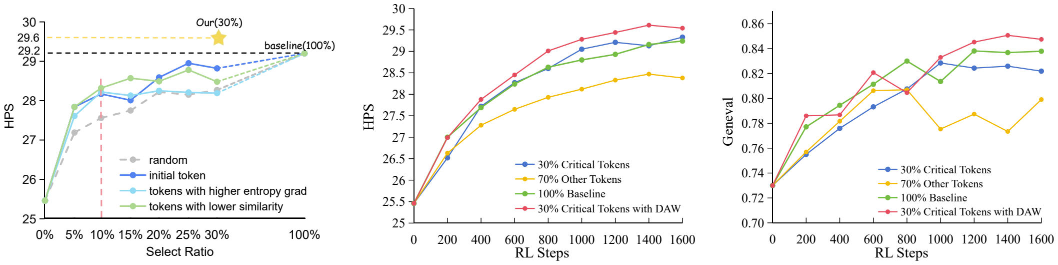

(a) Comparison on token selection strategies and selection ratios.

(b) Comparison of critical tokens and other tokens on HPS

(c) Comparison of critical tokens and other tokens on Geneval

Figure 7: (a): All three types of critical tokens deliver clear performance gains at 10% initial selection ratios and outperform random selection, with further increases yield only limited improvements. (b) & (c): GRPO with critical tokens (30%) has more performance improvement than GRPO with remaining tokens (70%). Our GCPO further achieves performance improvement. We further analyze the settings for the overall selection ratio and the selection ratio for each type in Appendix E.

6.3 Ablation Study

We conduct an analysis study on different token-selection strategies and selection rates, as shown in Fig. 7a. Within the initial selection ratios range (10% of tokens), GRPO performance rises rapidly (+2.81) with each of the three types of critical tokens, respectively; beyond this threshold, the gains are limited (+0.95). Moreover, combining all three types of critical tokens clearly outperforms selecting any single type at the same token budget (30% of tokens), which demonstrates the correct identification of critical tokens in RLVL training. We further verify that all three strategies significantly outperform random selection. As shown in Table 3, we present more experimental results on multiple benchmarks under Geneval and HPS reward settings. Our critical token strategies consistently achieve balanced performance improvements. Furthermore, with the introduction of dynamic advantage weight, all metrics reach optimal values, demonstrating the effectiveness of our designs.

Table 3: Ablation results on critical tokens and dynamic advantage weight. Init-T: initial tokens, HG-T: high entropy gradient tokens, LS-T: low similarity tokens; DAW: dynamic advantage weight.

Init-T	HG-T	LS-T	DAW	GenEval↑	T2I-CompBench						DEQA↑	HPS↑	ImgRwd↑
					Color↑	Shape↑	Texture↑	Spatial↑	Non-Spat.↑	Complex↑			
✓	-	-	-	0.82	0.6084	0.2820	0.3496	0.2374	0.2865	0.2877	3.66	28.90	0.63
-	✓	-	-	0.81	0.5440	0.2712	0.3368	0.2262	0.2832	0.2794	3.63	28.22	0.63
-	-	✓	-	0.82	0.6721	0.2942	0.4101	0.2569	0.2938	0.3109	3.64	28.78	0.66
✓	✓	✓	-	0.83	0.6602	0.2924	0.3991	0.2936	0.2943	0.3015	3.70	29.33	0.71
✓	✓	✓	✓	0.85	0.7373	0.3201	0.4803	0.3220	0.2948	0.3059	3.73	29.61	0.73

We also consider the comparison between 30% critical tokens and 70% of the remaining tokens. As shown in Fig. 7b and 7c, GRPO with critical tokens are comparable with the GRPO baseline, while GRPO with other tokens leads to a drop in performance. Despite the fact that the other tokens account for 70% of the total tokens used in training and more than twice the count of critical tokens, they still have a significant performance gap. This finding highlights the greater importance of critical tokens based on our selection strategy for effective model training.

In addition, to further illustrate the rationality of the selection ratio for each type and the overall selection ratio, we provide more experiments in the Appendix E. As shown in Table. 8, we observe that the imbalanced selection for each type significantly degrades performance compared to balanced selection (10%:10%:10%), which is also supported by the experimental results in Fig. 7a.

Notably, increasing the total selection ratios from 30% to 45% yields almost no performance improvement, but decreasing it from 30% to 15% results in a significant performance degradation, as shown in the Table. 10. Furthermore, increasing total selection ratios to the entire sequence of tokens leads to a decline in performance. This phenomenon arises from the use of DAW on the entire sequence of tokens, for which we conduct additional experiments and analyses in the Appendix E.4.

Next Token Prediction (NTP) is currently the most general paradigm in NLP and AR image generation. Nevertheless, based on the intrinsic spatial structure of images, previous works (Tian et al., 2024; Han et al., 2025; Ma et al., 2024) have explored next-scale prediction to achieve high-quality and efficient image generation. We successfully extend our method to the next-scale prediction generation paradigm. Specifically, we expand our method as follows: the importance of initial tokens (AR causality) is extended to the importance of early scales, while entropy-gradient-based structure and similarity-based diversity mechanisms can be seamlessly adapted. Our approach demonstrates strong generalizability and achieves superior performance to GRPO across multiple metrics. This suggests that the key concept of critical tokens is general and worthy of further investigation. **Notably, our GCPO utilizes only critical tokens (25% of the tokens).** The comparison results are shown in Table. 4 and Fig. 14.

Table 4: Results on scale-wise model. The best result is in green .

Method	DEQA↑	HPS↑	ImgReward↑	PickScore↑	GenEval↑
Star (Ma et al., 2024)	3.70	26.38	0.52	21.84	0.47
Star (Ma et al., 2024) + GRPO	4.11	30.17	0.76	22.19	0.50
Star (Ma et al., 2024) + GCPO (our)	4.15	30.32	0.78	22.17	0.49

7 Conclusion

In this paper, we introduce Group Critical-token Policy Optimization (**GCPO**), a novel RLVR framework for autoregressive image generation. We identify critical tokens in RLVR-based AR visual generation from three perspectives: Causal dependency of AR, Entropy-induced spatial structure, and RLVR-focused token diversity. We devise the dynamic advantage weight for critical tokens to enable reasonable exploration, based on their confidence divergence between the policy model and reference model. Extensive experiments demonstrate that by leveraging critical tokens (30% of the image tokens), GCPO achieves better performance than GRPO, which operates on the full tokens.

8 Acknowledgments

This work was supported by the Anhui Provincial Natural Science Foundation under Grant 2108085UD12. We acknowledge the support of GPU cluster built by MCC Lab of Information Science and Technology Institution, USTC. The AI-driven experiments, simulations and model training were performed on the robotic AI-Scientist platform of Chinese Academy of Sciences.

9 Ethics Statement

Data Usage. All training and evaluation datasets used in this study are publicly available and have been widely adopted in prior research, including Geneval, T2I-CompBench, DrawBench, and HPSv2. We do not collect or distribute any new human or proprietary data. The prompts and images used do not contain personally identifiable information or sensitive content.

Content and Bias. We do not introduce any new annotations or external knowledge sources that could inject additional biases beyond those already present in the original models and datasets. To further promote responsible use, we encourage the integration of existing safety filters, content-moderation tools, and bias-detection techniques when deploying models enhanced with our method.

10 Reproducibility Statement

Here, we provide content for better Reproducibility.

1. The detailed method is described in Sec. 5
2. Hyperparameters for all used models in this paper (see Sec. A).

Besides, all training data, checkpoints, and code will be released within the scope of the conference.

REFERENCES

James Betker, Gabriel Goh, Li Jing, Tim Brooks, Jianfeng Wang, Linjie Li, Long Ouyang, Juntang Zhuang, Joyce Lee, Yufei Guo, et al. Improving image generation with better captions. *Computer Science. https://cdn. openai. com/papers/dall-e-3. pdf*, 2(3):8, 2023.

L Lao Beyer, Tianhong Li, Xinlei Chen, Sertac Karaman, and Kaiming He. Highly compressed tokenizer can generate without training. *arXiv preprint arXiv:2506.08257*, 2025.

briaai. Rmbg v2.0 is a new state-of-the-art background removal model. `https://huggingface.co/briaai/RMBG-2.0/`, 2025.

Junsong Chen, Yue Wu, Simian Luo, Enze Xie, Sayak Paul, Ping Luo, Hang Zhao, and Zhenguo Li. Pixart-δ: Fast and controllable image generation with latent consistency models. *arXiv preprint arXiv:2401.05252*, 2024.

Xiaokang Chen, Zhiyu Wu, Xingchao Liu, Zizheng Pan, Wen Liu, Zhenda Xie, Xingkai Yu, and Chong Ruan. Janus-pro: Unified multimodal understanding and generation with data and model scaling. *arXiv preprint arXiv:2501.17811*, 2025a.

Xiwen Chen, Wenhui Zhu, Peijie Qiu, Xuanzhao Dong, Hao Wang, Haiyu Wu, Huayu Li, Aristeidis Sotiras, Yalin Wang, and Abolfazl Razi. Dra-grpo: Exploring diversity-aware reward adjustment for r1-zero-like training of large language models. *arXiv preprint arXiv:2505.09655*, 2025b.

Chaorui Deng, Deyao Zhu, Kunchang Li, Chenhui Gou, Feng Li, Zeyu Wang, Shu Zhong, Weihao Yu, Xiaonan Nie, Ziang Song, et al. Emerging properties in unified multimodal pretraining. *arXiv preprint arXiv:2505.14683*, 2025.

Patrick Esser, Robin Rombach, and Bjorn Ommer. Taming transformers for high-resolution image synthesis. In *Proceedings of the IEEE/CVF Conference on Computer Vision and Pattern Recognition*, pp. 12873–12883, 2021.

Patrick Esser, Sumith Kulal, Andreas Blattmann, Rahim Entezari, Jonas Müller, Harry Saini, Yam Levi, Dominik Lorenz, Axel Sauer, Frederic Boesel, et al. Scaling rectified flow transformers for high-resolution image synthesis. In *Forty-first International Conference on Machine Learning*, 2024.

Matteo Gallici and Haitz Sáez de Ocáriz Borde. Fine-tuning next-scale visual autoregressive models with group relative policy optimization. *arXiv preprint arXiv:2505.23331*, 2025.

Dhruba Ghosh, Hannaneh Hajishirzi, and Ludwig Schmidt. Geneval: An object-focused framework for evaluating text-to-image alignment. *Advances in Neural Information Processing Systems*, 36: 52132–52152, 2023.

Daya Guo, Dejian Yang, Haowei Zhang, Junxiao Song, Ruoyu Zhang, Runxin Xu, Qihao Zhu, Shirong Ma, Peiyi Wang, Xiao Bi, et al. Deepseek-r1: Incentivizing reasoning capability in llms via reinforcement learning. *arXiv preprint arXiv:2501.12948*, 2025a.

Ziyu Guo, Renrui Zhang, Chengzhuo Tong, Zhizheng Zhao, Rui Huang, Haoquan Zhang, Manyuan Zhang, Jiaming Liu, Shanghang Zhang, Peng Gao, et al. Can we generate images with cot? let's verify and reinforce image generation step by step. *arXiv preprint arXiv:2501.13926*, 2025b.

Jian Han, Jinlai Liu, Yi Jiang, Bin Yan, Yuqi Zhang, Zehuan Yuan, Bingyue Peng, and Xiaobing Liu. Infinity: Scaling bitwise autoregressive modeling for high-resolution image synthesis, 2024. *URL https://arxiv.org/abs/2412.04431*, 2025.

Andre He, Daniel Fried, and Sean Welleck. Rewarding the unlikely: Lifting grpo beyond distribution sharpening. *arXiv preprint arXiv:2506.02355*, 2025.

Yefei He, Feng Chen, Yuanyu He, Shaoxuan He, Hong Zhou, Kaipeng Zhang, and Bohan Zhuang. Zipar: Parallel auto-regressive image generation through spatial locality. *arXiv preprint arXiv:2412.04062*, 2024.

Jian Hu, Mingjie Liu, Ximing Lu, Fang Wu, Zaid Harchaoui, Shizhe Diao, Yejin Choi, Pavlo Molchanov, Jun Yang, Jan Kautz, et al. Brorl: Scaling reinforcement learning via broadened exploration. *arXiv preprint arXiv:2510.01180*, 2025.

Kaiyi Huang, Kaiyue Sun, Enze Xie, Zhenguo Li, and Xihui Liu. T2i-compbench: A comprehensive benchmark for open-world compositional text-to-image generation. *Advances in Neural Information Processing Systems*, 36:78723–78747, 2023.

Wenxuan Huang, Shuang Chen, Zheyong Xie, Shaosheng Cao, Shixiang Tang, Yufan Shen, Qingyu Yin, Wenbo Hu, Xiaoman Wang, Yuntian Tang, et al. Interleaving reasoning for better text-to-image generation. *arXiv preprint arXiv:2509.06945*, 2025.

Dongzhi Jiang, Ziyu Guo, Renrui Zhang, Zhuofan Zong, Hao Li, Le Zhuo, Shilin Yan, Pheng-Ann Heng, and Hongsheng Li. T2i-r1: Reinforcing image generation with collaborative semantic-level and token-level cot. *arXiv preprint arXiv:2505.00703*, 2025.

Yuval Kirstain, Adam Polyak, Uriel Singer, Shahbuland Matiana, Joe Penna, and Omer Levy. Pick-a-pic: An open dataset of user preferences for text-to-image generation. *Advances in Neural Information Processing Systems*, 36:36652–36663, 2023.

Black Forest Labs. Flux. `https://github.com/black-forest-labs/flux/`, 2024.

Bo Li, Yuanhan Zhang, Dong Guo, Renrui Zhang, Feng Li, Hao Zhang, Kaichen Zhang, Peiyuan Zhang, Yanwei Li, Ziwei Liu, et al. Llava-onevision: Easy visual task transfer. *arXiv preprint arXiv:2408.03326*, 2024.

Dacheng Li, Shiyi Cao, Tyler Griggs, Shu Liu, Xiangxi Mo, Eric Tang, Sumanth Hegde, Kourosh Hakhamaneshi, Shishir G Patil, Matei Zaharia, et al. Llms can easily learn to reason from demonstrations structure, not content, is what matters! *arXiv preprint arXiv:2502.07374*, 2025.

Zicheng Lin, Tian Liang, Jiahao Xu, Qiuzhi Lin, Xing Wang, Ruilin Luo, Chufan Shi, Siheng Li, Yujiu Yang, and Zhaopeng Tu. Critical tokens matter: Token-level contrastive estimation enhances llm's reasoning capability. *arXiv preprint arXiv:2411.19943*, 2024.

Dongyang Liu, Shitian Zhao, Le Zhuo, Weifeng Lin, Yi Xin, Xinyue Li, Qi Qin, Yu Qiao, Hongsheng Li, and Peng Gao. Lumina-mgpt: Illuminate flexible photorealistic text-to-image generation with multimodal generative pretraining. *arXiv preprint arXiv:2408.02657*, 2024a.

Jie Liu, Gongye Liu, Jiajun Liang, Yangguang Li, Jiaheng Liu, Xintao Wang, Pengfei Wan, Di Zhang, and Wanli Ouyang. Flow-grpo: Training flow matching models via online rl. *arXiv preprint arXiv:2505.05470*, 2025.

Shilong Liu, Zhaoyang Zeng, Tianhe Ren, Feng Li, Hao Zhang, Jie Yang, Qing Jiang, Chunyuan Li, Jianwei Yang, Hang Su, et al. Grounding dino: Marrying dino with grounded pre-training for open-set object detection. In *European Conference on Computer Vision*, pp. 38–55. Springer, 2024b.

Xiaoxiao Ma, Mohan Zhou, Tao Liang, Yalong Bai, Tiejun Zhao, Biye Li, Huaian Chen, and Yi Jin. Star: Scale-wise text-conditioned autoregressive image generation. *arXiv preprint arXiv:2406.10797*, 2024.

Xiaoxiao Ma, Haibo Qiu, Guohui Zhang, Zhixiong Zeng, Siqi Yang, Lin Ma, and Feng Zhao. Stage: Stable and generalizable grpo for autoregressive image generation. *arXiv preprint arXiv:2509.25027*, 2025.

OpenAI. Learning to reason with llms. `https://openai.com/index/learning-to-reason-with-llms/`, 2024.

OpenAI. Introducing 4o image generation. `https://openai.com/index/introducing-4o-image-generation/`, 2025.

Kaihang Pan, Wendong Bu, Yuruo Wu, Yang Wu, Kai Shen, Yunfei Li, Hang Zhao, Juncheng Li, Siliang Tang, and Yueting Zhuang. Focusdiff: Advancing fine-grained text-image alignment for autoregressive visual generation through rl. *arXiv preprint arXiv:2506.05501*, 2025a.

Kaihang Pan, Wang Lin, Zhongqi Yue, Tenglong Ao, Liyu Jia, Wei Zhao, Juncheng Li, Siliang Tang, and Hanwang Zhang. Generative multimodal pretraining with discrete diffusion timestep tokens. In *Proceedings of the IEEE/CVF Conference on Computer Vision and Pattern Recognition*, pp. 26136–26146, 2025b.

Yaning Pan, Qianqian Xie, Guohui Zhang, Zekun Wang, Yongqian Wen, Yuanxing Zhang, Haoxuan Hu, Zhiyu Pan, Yibing Huang, Zhidong Gan, et al. Mt-video-bench: A holistic video understanding benchmark for evaluating multimodal llms in multi-turn dialogues. *arXiv preprint arXiv:2510.17722*, 2025c.

Dustin Podell, Zion English, Kyle Lacey, Andreas Blattmann, Tim Dockhorn, Jonas Müller, Joe Penna, and Robin Rombach. Sdxl: Improving latent diffusion models for high-resolution image synthesis. *arXiv preprint arXiv:2307.01952*, 2023.

Aditya Ramesh, Prafulla Dhariwal, Alex Nichol, Casey Chu, and Mark Chen. Hierarchical text-conditional image generation with clip latents. *arXiv preprint arXiv:2204.06125*, 1(2):3, 2022.

Chitwan Saharia, William Chan, Saurabh Saxena, Lala Li, Jay Whang, Emily L Denton, Kamyar Ghasemipour, Raphael Gontijo Lopes, Burcu Karagol Ayan, Tim Salimans, et al. Photorealistic text-to-image diffusion models with deep language understanding. *Advances in Neural Information Processing Systems*, 35:36479–36494, 2022.

Claude E Shannon. A mathematical theory of communication. *The Bell system technical journal*, 27(3):379–423, 1948.

Zhihong Shao, Peiyi Wang, Qihao Zhu, Runxin Xu, Junxiao Song, Xiao Bi, Haowei Zhang, Mingchuan Zhang, YK Li, Yang Wu, et al. Deepseekmath: Pushing the limits of mathematical reasoning in open language models. *arXiv preprint arXiv:2402.03300*, 2024.

Vaishnavi Shrivastava, Ahmed Awadallah, Vidhisha Balachandran, Shivam Garg, Harkirat Behl, and Dimitris Papailiopoulos. Sample more to think less: Group filtered policy optimization for concise reasoning. *arXiv preprint arXiv:2508.09726*, 2025.

Peize Sun, Yi Jiang, Shoufa Chen, Shilong Zhang, Bingyue Peng, Ping Luo, and Zehuan Yuan. Autoregressive model beats diffusion: Llama for scalable image generation. *arXiv preprint arXiv:2406.06525*, 2024.

Chameleon Team. Chameleon: Mixed-modal early-fusion foundation models. *arXiv preprint arXiv:2405.09818*, 2024.

Kimi Team, Angang Du, Bofei Gao, Bowei Xing, Changjiu Jiang, Cheng Chen, Cheng Li, Chenjun Xiao, Chenzhuang Du, Chonghua Liao, et al. Kimi k1. 5: Scaling reinforcement learning with llms. *arXiv preprint arXiv:2501.12599*, 2025.

Keyu Tian, Yi Jiang, Zehuan Yuan, Bingyue Peng, and Liwei Wang. Visual autoregressive modeling: Scalable image generation via next-scale prediction. *Advances in Neural Information Processing Systems*, 37:84839–84865, 2024.

Shengbang Tong, David Fan, Jiachen Zhu, Yunyang Xiong, Xinlei Chen, Koustuv Sinha, Michael Rabbat, Yann LeCun, Saining Xie, and Zhuang Liu. Metamorph: Multimodal understanding and generation via instruction tuning. *arXiv preprint arXiv:2412.14164*, 2024.

Aaron Van Den Oord, Oriol Vinyals, et al. Neural discrete representation learning. *Advances in Neural Information Processing Systems*, 30, 2017.

Jean Vassoyan, Nathanaël Beau, and Roman Plaud. Ignore the kl penalty! boosting exploration on critical tokens to enhance rl fine-tuning. *arXiv preprint arXiv:2502.06533*, 2025.

Jiakang Wang, Runze Liu, Fuzheng Zhang, Xiu Li, and Guorui Zhou. Stabilizing knowledge, promoting reasoning: Dual-token constraints for rlvr. *arXiv preprint arXiv:2507.15778*, 2025a.

Jianfeng Wang, Zhengyuan Yang, Xiaowei Hu, Linjie Li, Kevin Lin, Zhe Gan, Zicheng Liu, Ce Liu, and Lijuan Wang. Git: A generative image-to-text transformer for vision and language. *arXiv preprint arXiv:2205.14100*, 2022.

Junke Wang, Zhi Tian, Xun Wang, Xinyu Zhang, Weilin Huang, Zuxuan Wu, and Yu-Gang Jiang. Simplear: Pushing the frontier of autoregressive visual generation through pretraining, sft, and rl. *arXiv preprint arXiv:2504.11455*, 2025b.

Qiuchen Wang, Ruixue Ding, Yu Zeng, Zehui Chen, Lin Chen, Shihang Wang, Pengjun Xie, Fei Huang, and Feng Zhao. Vrag-rl: Empower vision-perception-based rag for visually rich information understanding via iterative reasoning with reinforcement learning. *arXiv preprint arXiv:2505.22019*, 2025c.

Shenzhi Wang, Le Yu, Chang Gao, Chujie Zheng, Shixuan Liu, Rui Lu, Kai Dang, Xionghui Chen, Jianxin Yang, Zhenru Zhang, et al. Beyond the 80/20 rule: High-entropy minority tokens drive effective reinforcement learning for llm reasoning. *arXiv preprint arXiv:2506.01939*, 2025d.

Xinlong Wang, Xiaosong Zhang, Zhengxiong Luo, Quan Sun, Yufeng Cui, Jinsheng Wang, Fan Zhang, Yueze Wang, Zhen Li, Qiying Yu, et al. Emu3: Next-token prediction is all you need. *arXiv preprint arXiv:2409.18869*, 2024.

Xiaoshi Wu, Yiming Hao, Keqiang Sun, Yixiong Chen, Feng Zhu, Rui Zhao, and Hongsheng Li. Human preference score v2: A solid benchmark for evaluating human preferences of text-to-image synthesis. *arXiv preprint arXiv:2306.09341*, 2023.

Xunzhi Xiang and Qi Fan. Make it efficient: Dynamic sparse attention for autoregressive image generation. *arXiv preprint arXiv:2506.18226*, 2025.

Jinheng Xie, Weijia Mao, Zechen Bai, David Junhao Zhang, Weihao Wang, Kevin Qinghong Lin, Yuchao Gu, Zhijie Chen, Zhenheng Yang, and Mike Zheng Shou. Show-o: One single transformer to unify multimodal understanding and generation. *arXiv preprint arXiv:2408.12528*, 2024.

Jiazheng Xu, Xiao Liu, Yuchen Wu, Yuxuan Tong, Qinkai Li, Ming Ding, Jie Tang, and Yuxiao Dong. Imagereward: Learning and evaluating human preferences for text-to-image generation. *Advances in Neural Information Processing Systems*, 36:15903–15935, 2023.

Zeyue Xue, Jie Wu, Yu Gao, Fangyuan Kong, Lingting Zhu, Mengzhao Chen, Zhiheng Liu, Wei Liu, Qiushan Guo, Weilin Huang, et al. Dancegrpo: Unleashing grpo on visual generation. *arXiv preprint arXiv:2505.07818*, 2025.

An Yang, Anfeng Li, Baosong Yang, Beichen Zhang, Binyuan Hui, Bo Zheng, Bowen Yu, Chang Gao, Chengen Huang, Chenxu Lv, et al. Qwen3 technical report. *arXiv preprint arXiv:2505.09388*, 2025.

Hee Suk Yoon, Eunseop Yoon, Mark A Hasegawa-Johnson, Sungwoong Kim, and Chang D Yoo. Confpo: Exploiting policy model confidence for critical token selection in preference optimization. In *Forty-second International Conference on Machine Learning*, 2025.

Zhiyuan You, Xin Cai, Jinjin Gu, Tianfan Xue, and Chao Dong. Teaching large language models to regress accurate image quality scores using score distribution. In *Proceedings of the IEEE/CVF Conference on Computer Vision and Pattern Recognition*, pp. 14483–14494, 2025.

Hu Yu, Biao Gong, Hangjie Yuan, DanDan Zheng, Weilong Chai, Jingdong Chen, Kecheng Zheng, and Feng Zhao. Videomar: Autoregressive video generatio with continuous tokens. *arXiv preprint arXiv:2506.14168*, 2025a.

Hu Yu, Hao Luo, Hangjie Yuan, Yu Rong, and Feng Zhao. Frequency autoregressive image generation with continuous tokens. *arXiv preprint arXiv:2503.05305*, 2025b.

Jiahui Yu, Xin Li, Jing Yu Koh, Han Zhang, Ruoming Pang, James Qin, Alexander Ku, Yuanzhong Xu, Jason Baldridge, and Yonghui Wu. Vector-quantized image modeling with improved vqgan. *arXiv preprint arXiv:2110.04627*, 2021.

Qiying Yu, Zheng Zhang, Ruofei Zhu, Yufeng Yuan, Xiaochen Zuo, Yu Yue, Weinan Dai, Tiantian Fan, Gaohong Liu, Lingjun Liu, et al. Dapo: An open-source llm reinforcement learning system at scale. *arXiv preprint arXiv:2503.14476*, 2025c.

Shihao Yuan, Yahui Liu, Yang Yue, Jingyuan Zhang, Wangmeng Zuo, Qi Wang, Fuzheng Zhang, and Guorui Zhou. Ar-grpo: Training autoregressive image generation models via reinforcement learning. *arXiv preprint arXiv:2508.06924*, 2025.

Yu Yue, Yufeng Yuan, Qiying Yu, Xiaochen Zuo, Ruofei Zhu, Wenyuan Xu, Jiaze Chen, Chengyi Wang, TianTian Fan, Zhengyin Du, et al. Vapo: Efficient and reliable reinforcement learning for advanced reasoning tasks. *arXiv preprint arXiv:2504.05118*, 2025.

Yu Zeng, Wenxuan Huang, Shiting Huang, Xikun Bao, Yukun Qi, Yiming Zhao, Qiuchen Wang, Lin Chen, Zehui Chen, Huaian Chen, et al. Agentic jigsaw interaction learning for enhancing visual perception and reasoning in vision-language models. *arXiv preprint arXiv:2510.01304*, 2025a.

Yu Zeng, Yukun Qi, Yiming Zhao, Xikun Bao, Lin Chen, Zehui Chen, Shiting Huang, Jie Zhao, and Feng Zhao. Enhancing large vision-language models with ultra-detailed image caption generation. In *Proceedings of the 2025 Conference on Empirical Methods in Natural Language Processing*, pp. 26703–26729, 2025b.

Yu Zhang, Yunqi Li, Yifan Yang, Rui Wang, Yuqing Yang, Dai Qi, Jianmin Bao, Dongdong Chen, Chong Luo, and Lili Qiu. Reasongen-r1: Cot for autoregressive image generation models through sft and rl. *arXiv preprint arXiv:2505.24875*, 2025.

Yiming Zhao, Yu Zeng, Yukun Qi, YaoYang Liu, Xikun Bao, Lin Chen, Zehui Chen, Qing Miao, Chenxi Liu, Jie Zhao, et al. V2p-bench: Evaluating video-language understanding with visual prompts for better human-model interaction. *arXiv preprint arXiv:2503.17736*, 2025.

Chunting Zhou, Lili Yu, Arun Babu, Kushal Tirumala, Michihiro Yasunaga, Leonid Shamis, Jacob Kahn, Xuezhe Ma, Luke Zettlemoyer, and Omer Levy. Transfusion: Predict the next token and diffuse images with one multi-modal model. *arXiv preprint arXiv:2408.11039*, 2024.

A Detailed Experimental Setup

A.1 HyperParameter

In this paper, we used three models (LlamaGen (Sun et al., 2024), Janus-Pro 1B (Chen et al., 2025a), and Janus-Pro 7B (Chen et al., 2025a)) on the composition image task and image quality task. For different models and reward (HPS Reward (Wu et al., 2023) and Geneval Reward (Liu et al., 2025))settings, our training configuration and parameters are as follows:

Table 5: GCPO training hyperparameters.

Name	**LlamaGen for HPS**	**1B for Geneval**	**1B for HPS**	**7B for Geneval**	**7B for HPS**
Learning rate	1e-5	3e-6	1e-6	3e-6	1e-6
Beta β	0.04	0.01	0.01	0.01	0.01
Group Size G	8	4	4	4	8
Classifier-Free Guidance Scale	1	5	5	5	5
Max Gradient Norm	1.0	1.0	1.0	1.0	1.0
Batchsize	2	2	2	2	4
Training Steps	900	1,600	1,600	1,600	1,600
Gradient Accumulation Steps	2	1	1	1	1
Dynamic advantage weight clip ϵ_w	0.5	1	0.5	0.6	1
Image Resolution $h \times w$	256×256	384×384	384×384	384×384	384×384

A.2 Training efficiency

Compared with standard GRPO, our additional operations involve entropy gradient calculation and token embedding similarity computation. We have implemented certain optimizations, so these operations do not introduce additional computational burden or affect training efficiency.

B Entropy analysis in RLVR-based AR visual generation

In section 4.2, we discuss the entropy distribution of images in AR generation. We observe that the entropy distribution of image tokens exhibits a spatial pattern and fails to maintain consistency in different prompts. We further provide some examples and statistical results to illustrate this point, as shown in Fig. 8

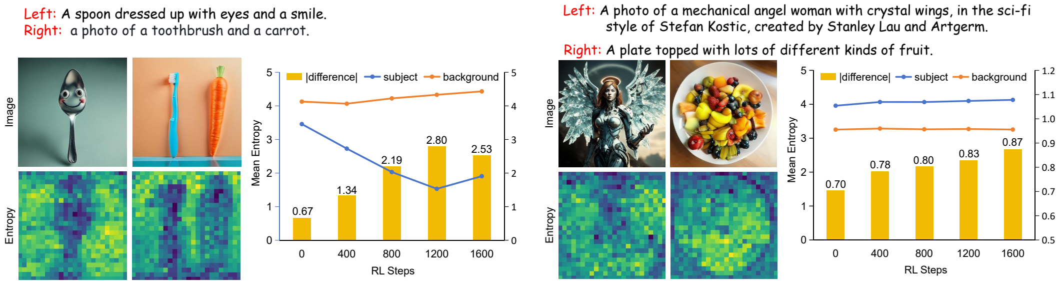

(a) The entropy distribution of simple or compositional prompts. The entropy of the background is significantly greater than that of the subject.

(b) The entropy distribution of complex or detailed prompts. The entropy of the subject is greater than that of the background.

Figure 8: In each figure, the blue line represents the average entropy of the subject regions, while the orange line represents the average entropy of the background regions. |difference| represents the average entropy difference between subject and background regions.

We argue that this entropy distribution is directly related to the complexity of the prompts. Specifically, for composition prompts, such as Geneval-style prompts, the entropy of the subject region is lower than that of the background region (see Fig. 8a). These prompts are relatively simple, including only the necessary keywords without excessive modifiers. As a result, the model has higher uncertainty when generating tokens in the background region due to the lack of sufficient prompt information. For complex prompts, such as the HPS testing data, the subject regions have a higher information density, resulting in higher entropy for tokens in these regions (see Fig. 8b).

Based on this insight, we conduct corresponding experiments to verify this point. We analyze the images generated by Janus-Pro and the corresponding entropy distribution, where prompts come from the Geneval Benchmark and HPS testing data. We use RMBG v2.0 (briaai, 2025), a state-of-the-art background removal model, to separate the foreground and background regions of the generated images. Then, we calculate the average token entropy within the foreground region, as shown in Fig. 8. The statistical results further verify our view.

In addition, we further investigate the evolution of entropy distribution during the RL training process. We find that RL training does not alter the original entropy pattern, but instead further reinforces it, which is similar to observations in LLMs (Li et al., 2025; Vassoyan et al., 2025). This phenomenon means that the entropy difference between the subject and background regions gradually increases (see the histogram in Fig. 8), resulting in more pronounced entropy (information) changes for high-gradient tokens in their neighborhood. Such information variation and complex structural regions are simultaneously coupled to these tokens, prompting us to include them in the scope of critical tokens for focused optimization.

C More Comparison Results with related work

In the field of AR image generation based on RLVR, (Jiang et al., 2025) and (Pan et al., 2025a) are representative works that are close to ours. The differences are that (Jiang et al., 2025) introduces semantic-CoT before image generation and uses a combination of multiple reward models, including HPS (Wu et al., 2023), GroundingDINO (Liu et al., 2024b), GIT (Wang et al., 2022), and LLaVA-OneVision-7B (Li et al., 2024), and constructs training data that includes both Geneval-style and T2i-compbench-style prompts. We only utilize Geneval rewards and Geneval-style data. (Pan et al., 2025a) constructs fine-grained paired prompt-image training data and first trains the model on paired data with images, then operates GRPO training without images. In contrast, we only perform image-free RL training. Comparison results on Geneval and T2i-compbench are shown in the Table 6. Our method achieves a significant lead on Geneval and also obtains comparable results on T2i-compbench.

Table 6: Comparison results with T2I-R1 and Focus-Diff on Geneval and T2I-CompBench.

Method↑	GenEval↑	T2I-CompBench					
		Color↑	Shape↑	Texture↑	Spatial↑	Non-Spat.↑	Complex↑
T2I-R1 (Jiang et al., 2025)	0.79	0.8130	0.5852	0.7243	0.3378	0.3090	0.3993
Focus-Diff (Pan et al., 2025a)	0.85	0.7996	0.5748	0.7007	0.3789	0.3098	0.3912
Janus-Pro-7B+GRPO	0.87	0.7478	0.3999	0.5849	0.2481	0.3090	0.3744
Janus-Pro-7B+GCPO	0.90	0.7508	0.5173	0.7030	0.3824	0.3133	0.3888

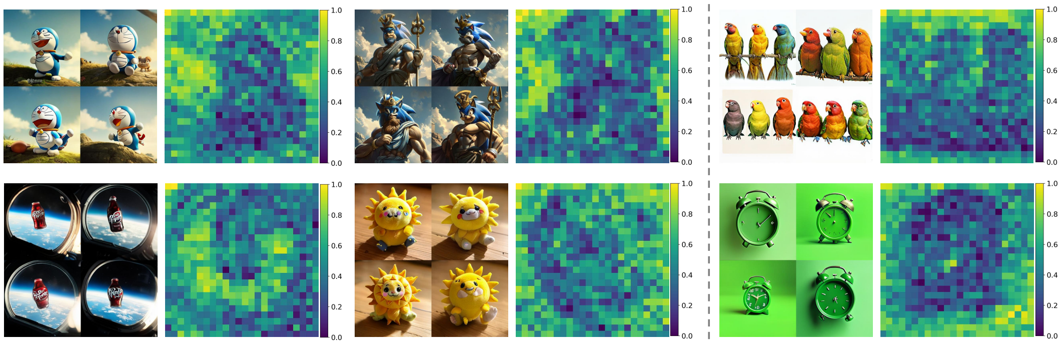

(a) complex prompts from HPS

(b) simple prompts from GenEval

Figure 9: Visual results from different benchmarks

D Analysis between similarity and regions in AR generation

We provide more examples from the HPS benchmark and GenEval benchmark to further illustrate the relationship between similarity and regions, as shown in the Fig. 9. It is obvious that simple background and texture regions in images within the same group tend to be more consistent (higher similarity), while complex regions show greater diversity (lower similarity).

E Additional Experiments

E.1 The influence of dynamic advantage weight

Dynamic Advantage Weight (DAW) is designed to work in cooperation with the critical token strategy and improve performance by further encouraging diverse advantages among the critical tokens. Applying DAW to all the 100% tokens may amplify certain negative gradients among the remaining non-critical tokens. To verify this, we conduct the corresponding experiments, as shown in Tabel. 7.

As shown in Table. 7, the experimental results show that our method (30% tokens with DAW) $>$ (100% tokens with DAW) $>$ (100% tokens without DAW). This verifies that 1) DAW is also useful to the general GRPO. 2) Critical tokens and DAW work synergistically to achieve the best performance. We argue that DAW may amplify certain negative gradients among the remaining non-critical tokens. Therefore, the rational selection of critical tokens is essential for performance improvement, and combining this selection with DAW leads to even better results.

Table 7: Ablation results on dynamic advantage weight

Method	DEQA↑	HPS↑	ImgReward↑	PickScore↑	GenEval↑
100% Tokens without DAW (GRPO)	3.67	29.16	0.73	21.59	0.84
100% Tokens with DAW	3.71	29.54	0.72	21.62	0.85
30% Critical Tokens without DAW	3.70	29.33	0.71	21.58	0.83
30% Critical Tokens with DAW (our)	3.73	29.61	0.73	21.60	0.85

E.2 Results on additional selection ratio settings

We further provide experiments with other selection ratios, as shown in Table 8. We observe that when the total selection ratio is 30%, and the selection ratio is set to 15%:10%:5%, the performance decreases significantly even though the total number of selected tokens remains unchanged.

We compare multiple ratios for each type of critical token, as shown in Fig. 7. For each type, 10% serves as a performance gain threshold. Beyond this point, performance improves slowly. Therefore, we adopt 10% as the default for each type.

Table 8: Comparison results on additional selection ratio settings

Method	DEQA↑	HPS↑	ImgReward↑	PickScore↑	GenEval↑
30% (15%:10%:5%)	3.66	29.54	0.62	21.54	0.83
30% (10%:10%:10%) (our)	3.73	29.61	0.73	21.60	0.85

E.3 The ablation on local averaging of the entropy map

Local averaging of the entropy map is proposed to reduce the noise and outliers in the entropy map, enabling more robust and efficient critical token selection. We further provide corresponding ablation experiments on this strategy in the Table. 9, where removing the local averaging results in a slight decrease in model performance.

Table 9: Comparison results on local averaging

Method	DEQA↑	HPS↑	ImgReward↑	PickScore↑	GenEval↑
w/o local averaging	3.71	29.56	0.71	21.58	0.84
w local averaging (our)	3.73	29.61	0.73	21.60	0.85

E.4 The ablation on the total selection proportion

In Table. 10, We provide experiments on the total selection proportion, including 15% (5%+5%+5%) and 45% (15%+15%+15%). We observe that reducing the selection proportion to 15% results in a significant performance drop, while further increasing it does not bring notable gains. Therefore, we outperform the GRPO with all tokens using as few critical tokens as possible.

Table 10: Ablation results on total selection proportion

Method	DEQA↑	HPS↑	ImgReward↑	PickScore↑	GenEval↑
15% (5%+5%+5%)	3.63	29.29	0.63	21.55	0.82
30% (10%+10%+10%) (our)	3.73	29.61	0.73	21.60	0.85
45% (15%+15%+15%)	3.70	29.65	0.75	21.62	0.85

E.5 The influence of group size

We argue that for the GRPO algorithm itself, a larger group size is empirically verified to yield more stable policy variance and a more diverse exploration space. Brorl (Hu et al., 2025) points out that substantially increasing the group size of the LLM can further improve the performance of models that are experiencing learning stagnation. Previous methods (Jiang et al., 2025; Zhang et al., 2025) typically set group size as a trade-off between performance and memory requirements.

To further validate this on AR visual generation, we provide more experiments of our method on different group sizes as shown in Table 11. We find that group size and HPS have a strong positive correlation. DEQA, PickScore, and ImageReward show significant improvements from 4 to 8, but the improvement is minimal when the group size is further increased (from 8 to 12). Conversely, the GenEval only shows an improvement when the group size increases (from 8 to 12).

Table 11: Comparison results on different group sizes

Method	GPU Memory↓	Training Time↓	DEQA↑	HPS↑	ImgReward↑	PickScore↑	Geneval↑
G=4	39G	4.5h	3.73	29.61	0.73	21.60	0.85
G=8	79G	9.2h	3.80	30.39	0.82	21.70	0.86
G=12	115G	11.4h	3.81	30.63	0.85	21.72	0.88

F More Visual Comparison Results

In this section, we further provide visual comparison results on the composition image task and image quality task to better illustrate the effectiveness and compatibility of our method. We will provide prompts for all images in Sec. F.5.

F.1 Comparison on LlamaGen

We only use the HPS Reward on LlamaGen and abandon the Geneval reward. This is because we find that the Geneval score for each image generated by LlamaGen is close to 0 and does not provide effective training rewards. Nevertheless, the model trained with the HPS reward not only demonstrates better generation quality, as shown in 10, but also further improves performance on Geneval.

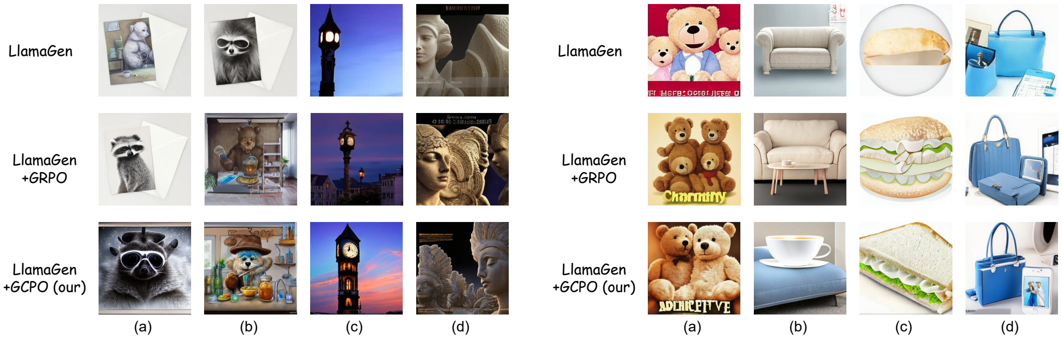

(a) Visual comparison results on HPS benchmark.

(b) Visual comparison results on Geneval

Figure 10: Qualitative comparison between the LlamaGen + GRPO and LlamaGen + GCPO (our) trained with HPS reward. Prompts are in Sec. F.5

F.2 Comparison on Janus-Pro 1B

We provide more qualitative comparison results on Janus-Pro 1B, as shown in 11 (HPS reward) and 12 (Geneval reward). These visual results further demonstrate the effectiveness of our approach.

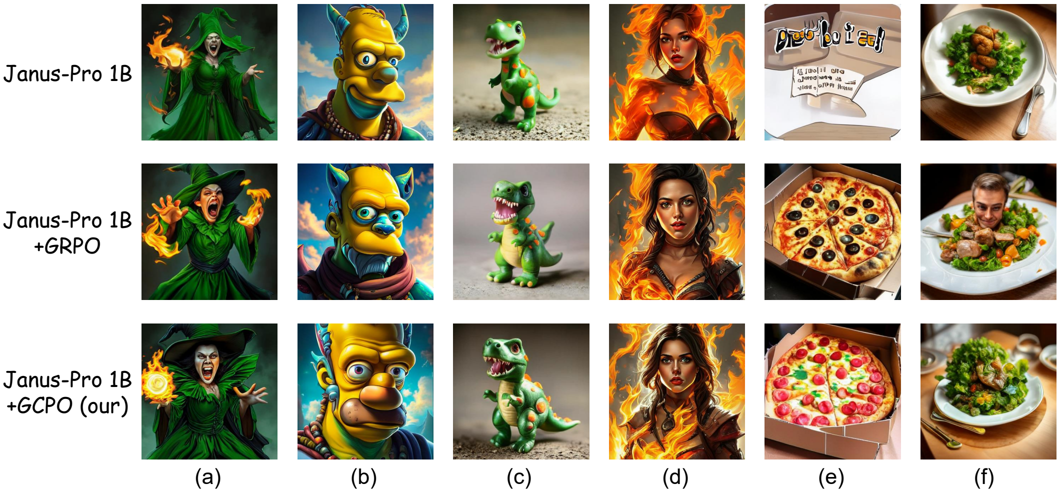

Figure 11: Qualitative comparison between the Janus-Pro 1B + GRPO and Janus-Pro 1B + GCPO (our) trained with HPS reward. Prompts are in Sec. F.5

F.3 More visual results during RLVR training

To better understand the training dynamics of our method, we visualize the results of samples generated by the same prompts during training, as shown in Fig. 13. These qualitative results intuitively demonstrate how the model continuously optimizes towards the goal of improving image quality and Human Preference Alignment as training progresses.

F.4 Comparison on Star

We provide more qualitative comparison results on the scale-wise model, Star (Ma et al., 2024), as shown in Fig. 14. These visual results further demonstrate the extension of our approach.

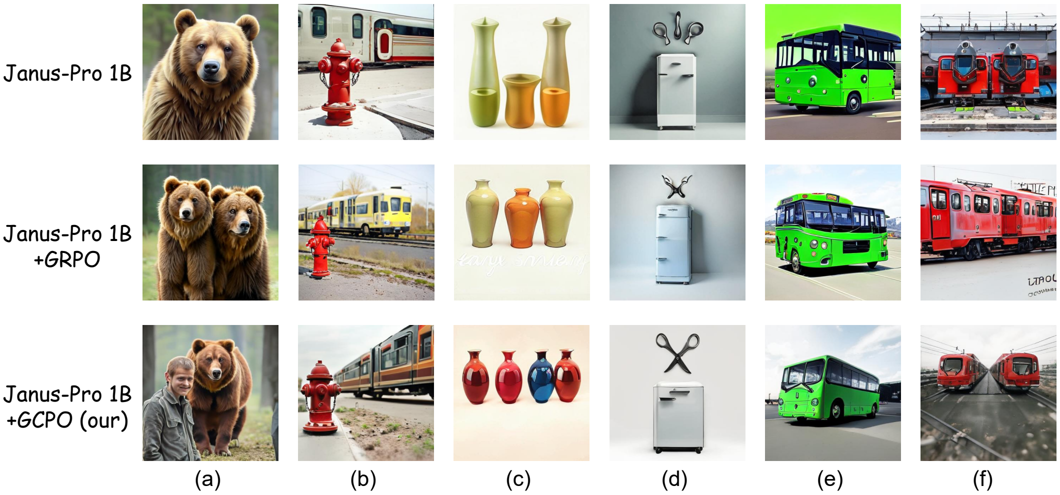

Figure 12: Qualitative comparison between the Janus-Pro 1B + GRPO and Janus-Pro 1B + GCPO (our) trained with Geneval reward. Prompts are in Sec. F.5

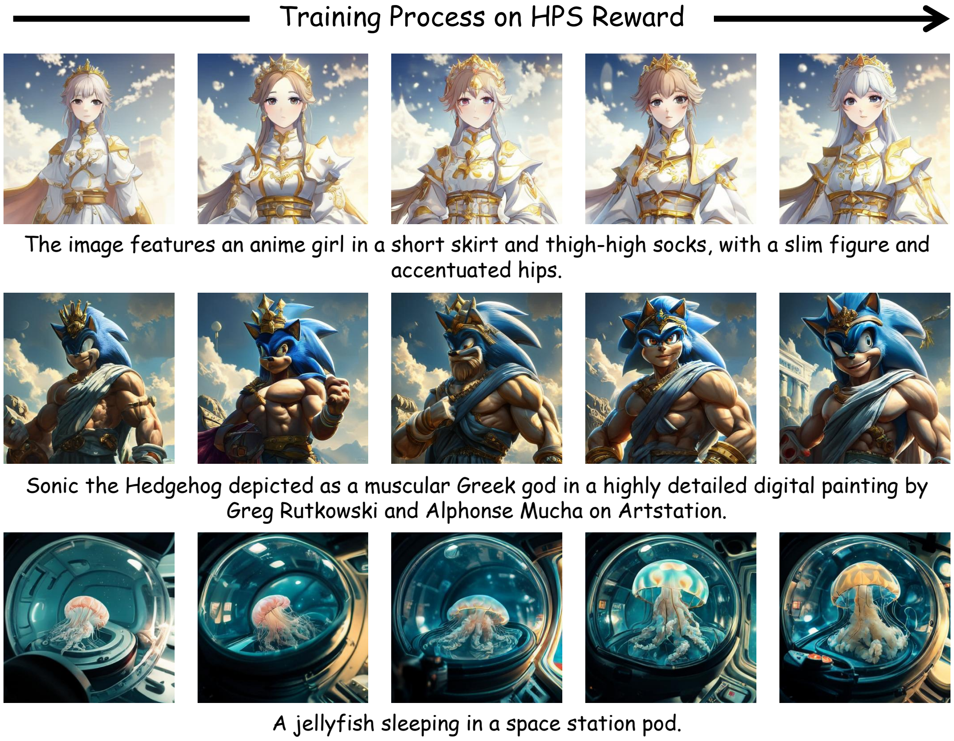
Training Process on HPS Reward
The image features an anime girl in a short skirt and thigh-high socks, with a slim figure and accentuated hips.
Sonic the Hedgehog depicted as a muscular Greek god in a highly detailed digital painting by Greg Rutkowski and Alphonse Mucha on Artstation.
A jellyfish sleeping in a space station pod.

Figure 13: We visualize the generated samples during the optimization of Janus-Pro 7B trained with HPS reward. As training progressed, the model is steadily optimized towards the target of Human Preference Alignment.

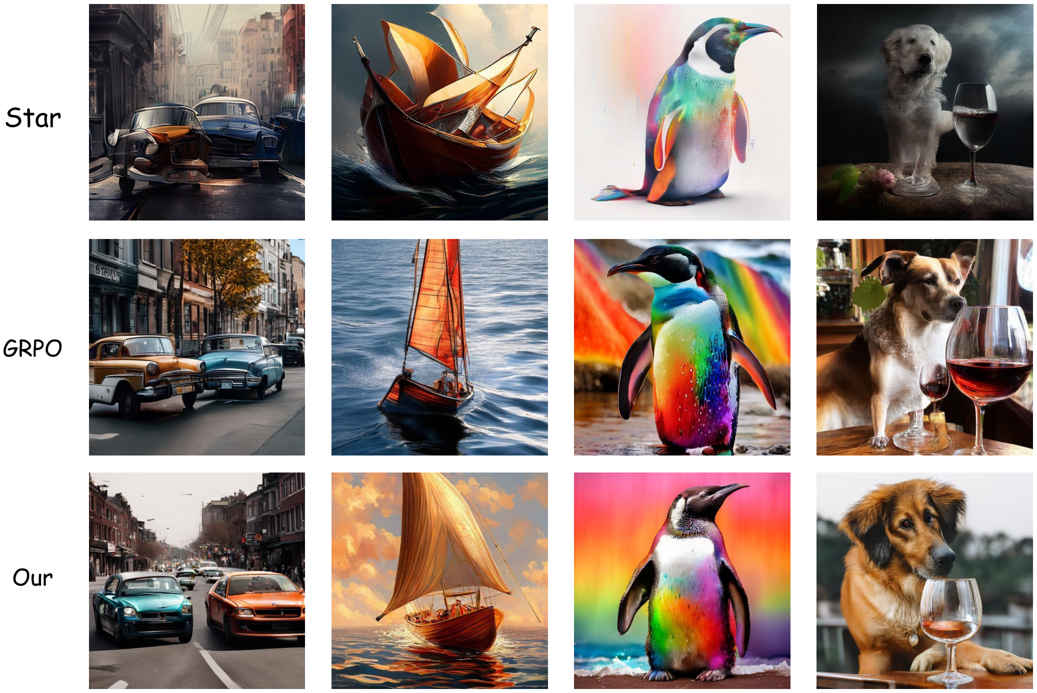

Figure 14: Visualization Results on Star.

F.5 Used prompts in this section

The prompts used in Fig. 10a are:

(a) The image is of a raccoon wearing a Peaky Blinders hat, surrounded by swirling mist and rendered with fine detail.

(b) A teddy bear mad scientist mixing chemicals depicted in oil painting style as a fantasy concept art piece.

(c) A clock tower with lighted clock faces, against a twilight sky.

(d) The image features a closeup portrait of stone angel statues, created with the Unreal Engine and featuring intricate details by various artists.

The prompts used in Fig. 10b are:

(a) a photo of two teddy bears

(b) a photo of a couch below a cup

(c) a photo of a white sandwich

(d) a photo of a blue handbag and a white cell phone

The prompts used in Fig. 11 are:

(a) Wicked witch casting fireball dressed in green with screaming expression.

(b) The image is a portrait of Homer Simpson as a Na'vi from Avatar, created with vibrant colors and highly detailed in a cinematic style reminiscent of romanticism by Eugene de Blaas and Ross Tran, available on Artstation with credits to Greg Rutkowski.

(c) A small green dinosaur toy with orange spots standing on its hind legs and roaring with its mouth open.

(d) Mila Kunis portrayed as a fire elemental in a highly detailed digital painting.

(e) A pizza is displayed inside a pizza box.

(f) A portrait of a dinner dish of a protein and greens.

The prompts used in Fig. 12 are:

(a) a photo of a person and a bear

(b) a photo of a fire hydrant and a train

(c) a photo of four bowls

(d) a photo of a baseball glove right of a bear

(e) a photo of a green bus

(f) a photo of two trains

G THE USE OF LARGE LANGUAGE MODELS (LLMS)

In this paper, LLMs are employed to refine the writing, further enhancing the readability and quality of the paper.